



# Interannual variability of the seesaw mode of the interface between the Indian and East Asian summer monsoons

Ruowen Yang<sup>1</sup> · Jian Wang<sup>1</sup>

Received: 3 September 2018 / Accepted: 25 January 2019 / Published online: 30 January 2019  
© Springer-Verlag GmbH Germany, part of Springer Nature 2019

## Abstract

The relation between the seesaw mode of the Interface between the Indian summer monsoon and East Asian summer monsoon (IIE) and the South China Sea summer monsoon trough (SCSSMT) and the Indian summer monsoon trough (ISMT) is investigated using two atmospheric reanalyses together with outgoing longwave radiation, sea surface temperature (SST), and gridded precipitation datasets. Canonical correlation analysis combined with empirical orthogonal functions, correlation, and composite analysis are employed. Results indicate that a stronger ISMT and SCSSMT resulting from colder SST over the tropical Indian Ocean and tropical east-central Pacific cause the IIE to deviate from its normal position in an anti-clockwise direction, with a node at around 22°N. This leads to heavier than normal summer rainfall over the north-central Indian subcontinent and South China Sea, but weaker than normal from the low and middle reaches of the Yangtze River and South Korea to central Japan. A weaker ISMT and SCSSMT resulting from warmer SST over the tropical Indian Ocean and tropical east-central Pacific causes the IIE to deviate from its normal position in a clockwise direction, and the anomalous summer rainfall pattern is the opposite of that for the stronger troughs. Further analysis indicates that the SCSSMT plays a crucial role in the evolution of the IIE seesaw mode. The latitudinal difference between the IMST and SCSSMT may be one of the most important reasons for the formation of the IIE seesaw mode.

## 1 Introduction

The Indian summer monsoon (ISM) and East Asian summer monsoon (EASM) are both part of the Asian summer monsoon (ASM), which is the most complex and powerful monsoon system in the world. These two subsystems are mutually independent to some extent, but otherwise are known to interact with each other (e.g., Jin and Chen 1982; Zhu et al. 1986; Tao et al. 2016; Kang et al. 1999; Jin et al. 2013; Krishnamurthy 2016). Because the South China Sea summer monsoon (SCSSM) is the tropical part of the EASM (Tao et al. 2016; Ding et al. 2004), the ASM variability can be represented by the variability of the South China Sea summer monsoon trough (SCSSMT), located around the region 15°–25°N, 70°–95°E and the Indian summer monsoon trough (ISMT), located around the area 10°–20°N, 105°–120°E. For example, both troughs feature a tropical convergence zone. The ISMT is formed by

the warmer and wetter southwesterly flow from the Indian Ocean and Southern Hemisphere that turns southeasterly along the foothills of the Himalayas. The SCSSMT is formed by the warmer and wetter southwesterly flow from the Bay of Bengal that converges with easterly flow at the southern edge of the western North Pacific subtropical high (WPSH) (Krishnamurti and Bhalme 1976; Tao et al. 2016; Wang and Wu 1997; He et al. 2000; Lim et al. 2002; Pan and Li 2006).

As the ISM and EASM are mutually independent to some extent and adjacent to each other, there should be an interface between them. In an early study by Jin and Chen (1982), it was suggested that the interface between the ISM and EASM (hereafter abbreviated to the IIE) is normally found between 95°E and 100°E. Later, Wang and Lin (2002) and Wang et al. (2003) indicated that the IIE is located at approximately 105°E. More recently, Cao et al. (2012) objectively and quantitatively defined the IIE using equivalent potential temperature and concluded that the IIE is located at around 100°E. They also investigated the existence of a relationship between the IIE and the intensity of the ISM and EASM. Specifically, the IIE will shift farther east than normal under a strong EASM and weak ISM, but

✉ Ruowen Yang  
yangruowen@ynu.edu.cn

<sup>1</sup> Department of Atmospheric Sciences, Yunnan University, Kunming 650091, China

move farther west than normal under the opposite conditions. The WPSH plays an important role in the interannual variability of the IIE (Tao et al. 2016). So, a better understanding of IIE variability and its climatic effects may improve the accuracy of seasonal forecasts of the ASM from a new perspective.

From the above-mentioned studies, as well as Fig. 1 in the present study, we can see that the IIE is also present between the SCSSMT and ISMT. This suggests that the variability of the SCSSMT and ISMT may be closely related to IIE variability. However, few studies have addressed the covariant modes of the IIE, SCSSMT, and ISMT and they remain to be elucidated. In the present study, a diagnosis of observations suggests that the activity of the SCSSMT and ISMT plays one of the most important roles in IIE variability. Section 2 describes the datasets and methods. Section 3 investigates the covariant modes of the IIE, SCSSMT, and ISMT, the relationship between the covariant modes and summer rainfall over the Asian monsoon region, and the relative contribution of the SCSSMT and ISMT to the IIE variability. A summary is provided in Sect. 4.

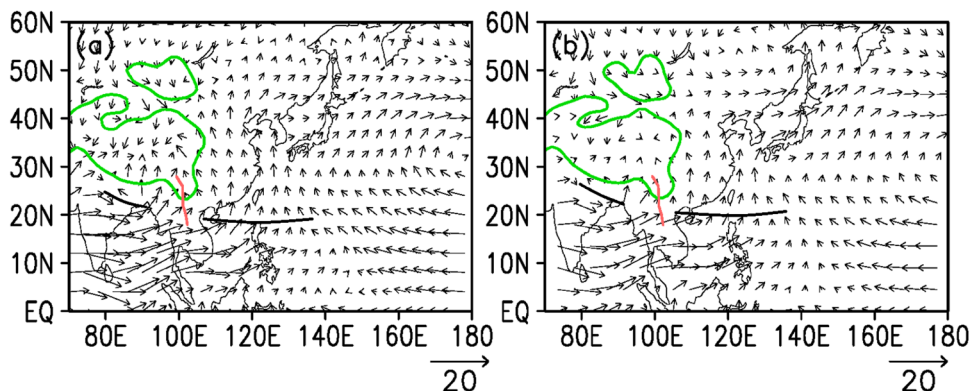
## 2 Data and methods

We use twentieth century reanalysis data (version 2, hereafter referred to as NOAA-V2) and outgoing longwave radiation (OLR) data provided by NOAA/OAR/ESRL PSD, and ERA-Interim reanalysis data (hereafter referred to as ERA-Interim) provided by the ECMWF for the summers (June–July–August; JJA) of 1981–2010 (Liebmann 1996; Whitaker et al. 2004; Compo et al. 2006, 2011; Dee et al. 2011). The resolutions of NOAA-V2, the OLR data and ERA-Interim are  $2^\circ$ ,  $2.5^\circ$  and  $2^\circ$  (for both latitude and longitude), respectively. The reanalysis data include horizontal wind at 850 hPa, sea level pressure (SLP), and relative vorticity at 850 hPa. We also use APHRODITE

(Asian Precipitation—Highly Resolved Observational Data Integration Towards Evaluation of Water Observational Data Integration Towards Evaluation of Water) gridded precipitation data with  $0.25^\circ$  resolution (Yatagai et al. 2012) and sea surface temperature (SST) data provided by the Met Office Hadley Center (Kennedy et al. 2011a, b) with  $1^\circ$  resolution. The IIE is defined as where the zonal gradient of equivalent potential temperature is equal to zero at around  $100^\circ\text{E}$ . The mathematical meaning is the extremum of the equivalent potential temperature over the saddle-shaped distribution in this region. The physical meaning of the IIE is that the summer monsoonal air masses from the Bay of Bengal and South China Sea mix at the extremum of equivalent potential temperature, and the two monsoonal air masses cannot be discriminated from each other. The climatological IIE is located along  $18^\circ\text{N}$ ,  $102.98^\circ\text{E}$  at 900 hPa,  $20^\circ\text{N}$ ,  $101.68^\circ\text{E}$  at 850 hPa,  $22^\circ\text{N}$ ,  $100.88^\circ\text{E}$  at 800 hPa,  $24^\circ\text{N}$ ,  $100.96^\circ\text{E}$  at 750 hPa,  $26^\circ\text{N}$ ,  $101.08^\circ\text{E}$  at 650 hPa, and  $28^\circ\text{N}$ ,  $99.32^\circ\text{E}$  at 600 hPa (Cao et al. 2012). The corresponding IIE series used in this paper are the same as those in Cao et al. (2012). The domain of interest of atmospheric circulation in this paper is  $0^\circ$ – $60^\circ\text{N}$ ,  $70^\circ\text{E}$ – $180^\circ$ .

Canonical correlation analysis (CCA) and corresponding chi-squared tests are extensively used to find the optimum linear combination of two multidimensional vectors (e.g., Barnett and Preisendorfer 1987; von Storch et al. 1993; Heyen et al. 1996; Busuioc et al. 2006, 2008). Because the pairs of patterns selected by CCA are spatially and temporally dependent variables, their corresponding time series are optimally correlated. Before applying CCA, the variables are generally projected onto their empirical orthogonal functions (EOF) to decrease the dimensionality of the data space. Such an analysis method is therefore called the EOF-CCA method. Other methods used here include correlation analysis, composite analysis, and corresponding Student's *t*-tests.

**Fig. 1** Climatological horizontal winds (units:  $\text{m s}^{-1}$ ) at 850 hPa calculated from **a** NOAA-V2 and **b** ERA-Interim. The thick black line denotes the summer monsoon troughs. The red solid line is the IIE. The green line denotes terrain



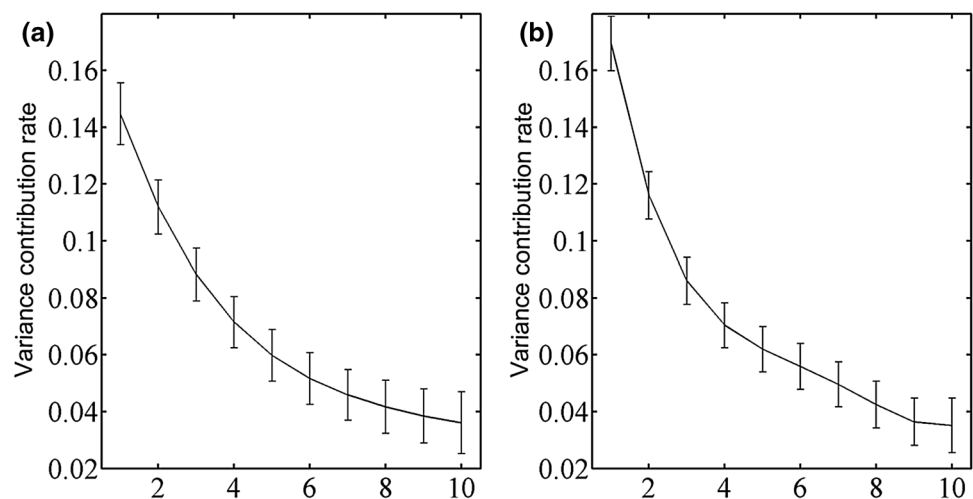
### 3 Results

#### 3.1 EOF-CCA results for the relationship between the IIE and two summer troughs

The 850 hPa horizontal wind field is generally adopted to study the variability of the summer monsoon (e.g., Webster et al. 1998; Wang 2006; Krishnamurti et al. 2013). However, the grid size of the horizontal wind field (1736 grid cells), is much larger than the length of the time period (30 a), we first performed EOF analysis on the 850 hPa zonal and meridional winds of NOAA-V2 over  $0^{\circ}$ – $60^{\circ}$ N,  $70^{\circ}$ E– $180^{\circ}$ . Figure 2a shows that the first three eigenvalues whose explained variance reach 34.5% can be separated from each other. So, the time series associated with the top three eigenvalues were chosen as the right field. Given the IIE data at six latitudes from  $18^{\circ}$ N to  $28^{\circ}$ N as the left field, the CCA was performed. The chi-squared test values of the first three canonical correlation fields were 34.9, 15.2 and 2.4, respectively. Only the first canonical correlation field passed the significance test at the 99% confidence level, while the remaining two did not pass the significance test even at the 90% confidence level. Here, we only need to analyze the first canonical correlation field. Figure 3a shows that the IIE presents a seesaw mode with a latitudinal node at  $22^{\circ}$ N. Because the anomalies of the IIE at  $18^{\circ}$ N,  $24^{\circ}$ N,  $26^{\circ}$ N, and  $28^{\circ}$ N passed the significance test at the 95% confidence level, it is clear that the IIE shifts farther east (west) than normal at  $18^{\circ}$ N, shifts little between  $20^{\circ}$ N and  $22^{\circ}$ N, and conspicuously shifts farther west (east) than normal north of  $22^{\circ}$ N when the time series of the right CCA field changes by  $\pm 1$  unit. Focusing on the 850 hPa horizontal wind anomalies associated with the IIE seesaw mode, we can see that there are three anomalous wind belts over the study

domain: an anomalous westerly belt that mainly appears south of  $20^{\circ}$ N and within  $70^{\circ}$ E– $180^{\circ}$ ; another at approximately  $40^{\circ}$ – $50^{\circ}$ N,  $120^{\circ}$ – $160^{\circ}$ E; and an anomalous easterly belt at around  $20^{\circ}$ – $30^{\circ}$ N,  $80^{\circ}$ E– $180^{\circ}$  lying between these two westerly belts (Fig. 3b). The configuration of the two anomalous wind belts south of  $30^{\circ}$ N, which directly results in two cyclonic anomalies over the rectangles C1 and C2 shown in Fig. 3e, implies that monsoon troughs are stronger than normal over India and the South China Sea. Because the correlation coefficient between the time series of the left canonical correlation field and right canonical correlation field reaches 0.75, passing the significance test at the 99% confidence level (Fig. 3c), there is significant positive correlation between the left and right canonical correlation fields. We repeated the EOF-CCA, but substituted the 850 hPa horizontal wind field of ERA-Interim for that of NOAA-V2. Figure 2b shows that the first three eigenvalues can also be separated from each other, and the corresponding explained variance reached 36.9%, similar to the explained variance associated with NOAA-V2. Choosing the time series associated with the top three eigenvalues as the right field and the same IIE data at six latitudes from  $18^{\circ}$ N to  $28^{\circ}$ N as the left field, the CCA was performed again. The Chi square test values of the first three canonical correlation fields were 36.1, 17.7, and 5.3, respectively. Similarly to the significance test results for NOAA-V2, only the first canonical correlation field passed the significance test at the 99% confidence level. So, we only show the first canonical correlation field. A seesaw mode with a latitudinal node at around  $22^{\circ}$ N can also be seen in Fig. 3d. The IIE anomalies also pass the significance test at the 95% confidence level at  $18^{\circ}$ N,  $24^{\circ}$ N,  $26^{\circ}$ N, and  $28^{\circ}$ N. Two significant cyclonic anomalies can be observed at around  $10^{\circ}$ – $22^{\circ}$ N,  $108^{\circ}$ – $120^{\circ}$ E and  $16^{\circ}$ – $26^{\circ}$ N,  $76^{\circ}$ – $96^{\circ}$ E (Fig. 3e). The correlation coefficient between the time series of the left and right canonical

**Fig. 2** The North test for the first 10 eigenvalues of horizontal winds calculated from **a** NOAA-V2 and **b** ERA-Interim



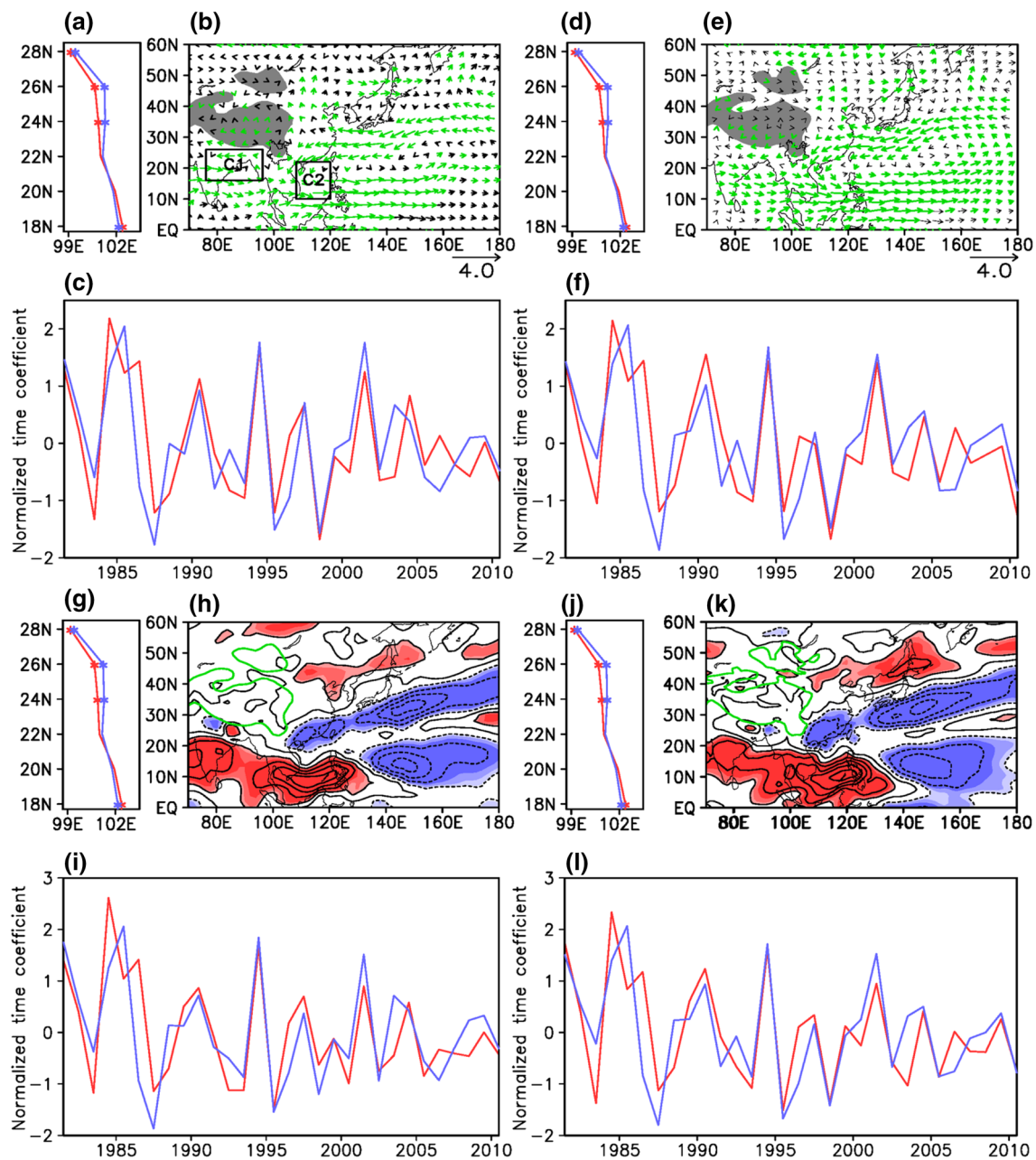


**Fig. 3** First mode of the EOF-CCA analysis of **a** the position of the IIE and **b** 850-hPa horizontal winds (units:  $\text{m s}^{-1}$ ). **c** Time series of the IIE (blue line) and 850-hPa horizontal winds (red line). The results in **a–c** are calculated using NOAA-V2, and **d–f** are the same as **a–c** but calculated using ERA-Interim. **g–i** are the same as **a–c** but calculated using 850-hPa total wind. **j–l** are the same as **d–f** but calculated using 850-hPa total wind. The red (blue) line in **a**, **d**, **g** and

**j** denotes the position of the IIE associated with positive (negative) anomalies of the CCA field. The asterisks in **a**, **d**, **g**, **j** denote the values passing the significance test at the 95% confidence level. Shaded areas in **b**, **e** and green lines in **h**, **k** denote terrain, and the green vectors are values passing the significance test at the 95% confidence level. C1 and C2 denote the climatological position of the ISMT and ISMT, respectively

correlation fields (0.74) passes the significance test at the 99% confidence level (Fig. 3f), also suggesting that there is a significant positive correlation between the left and the right canonical correlation fields. In fact, the correlation coefficients between the two time series of the left canonical correlation fields (the blue lines in Fig. 3c, f),

and between the two time series of the right canonical correlation fields (the red lines in Fig. 3c, f) are 0.98 and 0.97. If 850-hPa total wind is adopted in the CCA analysis (g–i, j–l), the results are consistent with those associated with the 850-hPa horizontal winds. Herein, the correlation coefficients between the two time series of the left

canonical correlation fields (the blue lines in Fig. 3c, i), and between the two time series of the right canonical correlation fields (the red lines in Fig. 3c, i) are 0.97 and 0.95. Those calculated using ERA-Interim are 0.99 (the blue lines in Fig. 3f, l) and 0.96 (the red lines in Fig. 3f, l). The stronger winds around 6°–20°N, 70°–120°E and weaker winds around 20°–30°N, 110°–140°E will result in the IIE shifting westward north of 22°N, but eastward south of 22°N. Figure 3d–f, j–l show the same patterns as Fig. 3a–c, g–i, respectively. These results suggest that the results obtained by the two reanalysis datasets and different variables are consistent, and further indicate that there is a significant relationship between the IIE, ISMT and SCSSMT. When the ISMT and SCSSMT are stronger than normal, the IIE shifts westward north of the seesaw node (22°N), but eastward south of 22°N. When the ISMT and SCSSMT are weaker than normal, the opposite conditions occur.

### 3.2 Composite results for the relationship between the IIE and two summer troughs

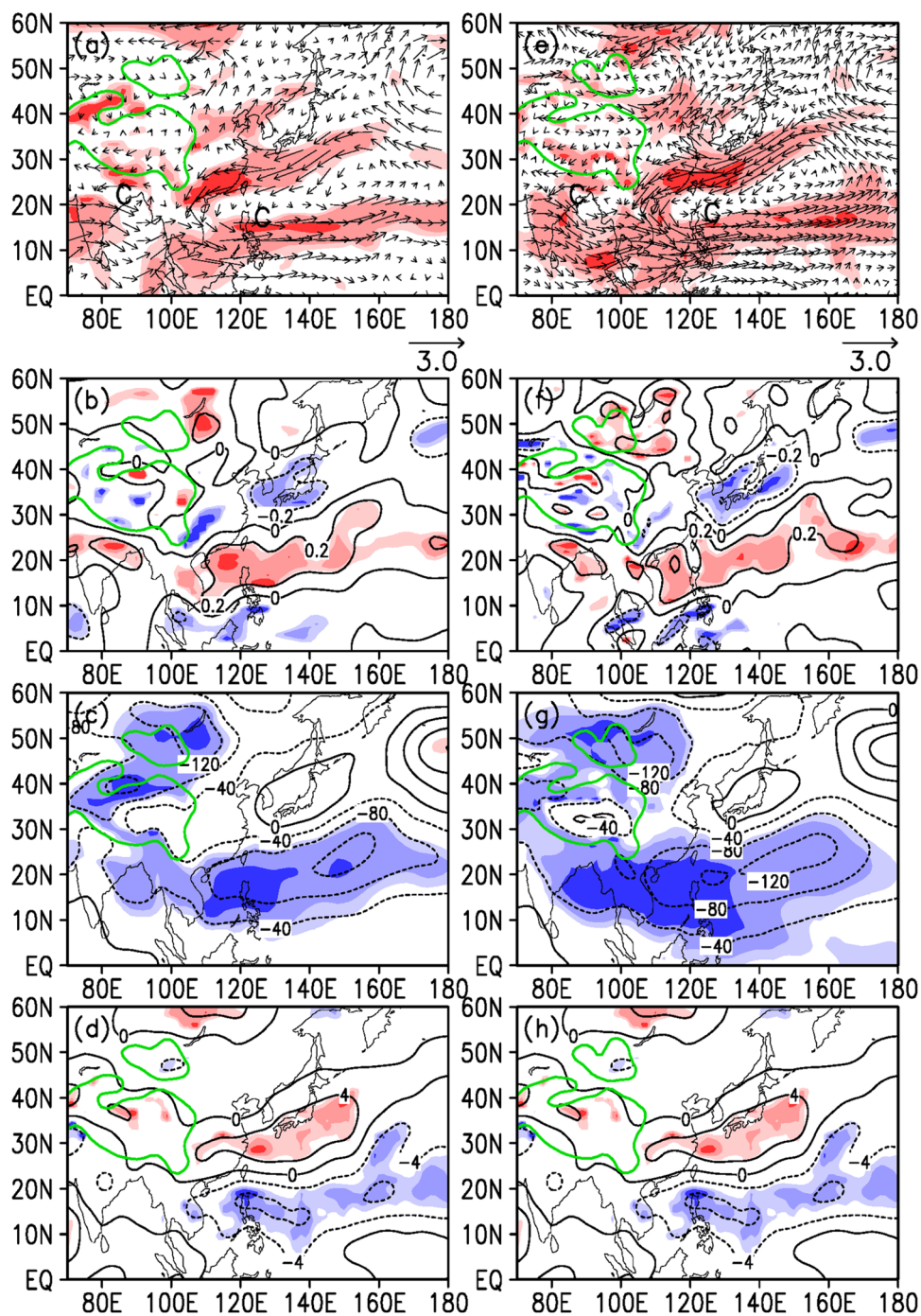
To verify the relationship between the IIE and the monsoon troughs revealed by EOF-CCA, we performed a composite analysis of the IIE, horizontal wind at 850 hPa, SLP, relative vorticity at 850 hPa, and the OLR over the study domain with the two atmospheric reanalysis datasets. We defined positive-anomaly years using the criterion that the value of the time series (red line in Fig. 3c, f) associated with the right canonical correlation field (horizontal winds) is larger than 1.0 standard deviation. Seven years were identified as positive-anomaly years in both atmospheric reanalysis datasets: 1981, 1984, 1985, 1986, 1990, 1994, and 2001.

Figure 4a shows the positive-anomaly 850-hPa winds associated with NOAA-V2. There is a strong resemblance between Figs. 3b and 4a. Their spatial correlation coefficient is 0.84, passing the significance test above the 99% confidence level. Significant cyclonic anomalies appear around two regions: one at 20°–30°N, 70°–96°E, and the other at 10°–20°N, 110°–160°E. The relative vorticity anomalies at 850 hPa (Fig. 4b), the SLP anomalies (Fig. 4c) and the OLR anomalies (Fig. 4d) agree well with the horizontal wind anomalies at 850 hPa. The positive relative vorticity anomalies appear in the same two regions, with center values of about  $0.2 \times 10^{-5} \text{ s}^{-1}$  that pass the significance test at the 95% confidence level (Fig. 4b). The negative SLP anomalies occur in almost the same two regions, with values below  $-40 \text{ Pa}$  and passing the significance test at the 95% confidence level (Fig. 4c). The negative OLR anomalies also occur around the same two regions; those around the SCS have center values of below  $-8 \text{ W m}^{-2}$  and pass the significance test at the 95%

confidence level, while those around north-central India are relatively modest (Fig. 4d). These mutually consistent results suggest that the ISMT and SCSSMT are significantly stronger than normal in positive-anomaly years. Comparing Fig. 4a–d with e–g, calculated using ERA-Interim, we can see that the positions and corresponding magnitudes of atmospheric circulation anomalies, especially the anomalous ISMT and SCSSMT, are similar to each other in positive-anomaly years. The atmospheric circulation anomalies calculated from ERA-Interim are more conspicuous, with larger areas passing the significance test above the 90% confidence level in comparison with those calculated from NOAA-V2. In relation to these anomalies, the IIE shifts westward in the area north of 22°N and eastward in the area south of 20°N; the westward movements at 24°N and 26°N are the most significant because the differences between the anomalies and the mean pass the significance test at the 95% confidence level (Fig. 6a, c).

Negative-anomaly years are defined as having time series values less than  $-1.0$  times the standard deviation. This defines 4 years (1983, 1987, 1995 and 1998) in both the NOAA-V2 and ERA-Interim datasets and an additional 2 years (1993 and 2010) in ERA-Interim. Figure 5a–d, calculated from NOAA-V2, almost mirror the anomalous patterns in Fig. 4a–d. The spatial correlation coefficients between them are  $-0.70$ ,  $-0.66$ ,  $-0.73$ ,  $-0.62$  for horizontal winds at 850 hPa, relative vorticity at 850 hPa, SLP and OLR, respectively. All correlation coefficients pass the significance test above the 99% confidence level. Figure 5e–h (ERA-Interim) mirror Fig. 4e–h, and resemble Fig. 5a–d but with a larger area passing the significance test above the 90% confidence level. The spatial correlation coefficients between Figs. 4e–h and 5e–h are  $-0.79$ ,  $-0.68$ ,  $-0.68$ , and  $-0.70$  for horizontal winds at 850 hPa, relative vorticity at 850 hPa, SLP, and OLR, respectively. All correlation coefficients pass the significance test above the 99% confidence level. These consistent results suggest that the ISMT and SCSSMT are significantly weaker than normal in negative-anomaly years. It is also clear that the seesaw pattern of the IIE as calculated from these anomalies follows that in Fig. 3a, d (Fig. 6b, d). This confirms the result that the IIE shifts eastward in the area north of 22°N and westward in the area south of 20°N, respectively (the blue lines in Fig. 3a, d). These composite analysis results obtained using the two reanalysis datasets are consistent, and also agree with the EOF-CCA results, indicating that there is a true seesaw mode of the IIE closely associated with the ISMT and SCSSMT. When the two summer monsoon troughs over India and the SCS are stronger (weaker) than normal, the IIE shifts westward (eastward) in the area north of 22°N and eastward (westward) in the area south of 22°N.

**Fig. 4** Composite anomalies of summer (JJA) mean **a** horizontal winds at 850 hPa (units:  $\text{m s}^{-1}$ ), **b** relative vorticity at 850 hPa (units:  $10^{-5} \text{ s}^{-1}$ ), **c** SLP (units: Pa) and **d** OLR (units:  $\text{W m}^{-2}$ ) in positive-anomaly years of horizontal winds. The areas shaded from light to dark red/blue denote correlation coefficients passing the significance test at the 90%, 95% and 99% confidence level, respectively. The green line denotes topography. The results in **a–d** are calculated using NOAA-V2, and **e–h** are the same as **a–d** but calculated using ERA-Interim. Centers of the anomalous cyclones are shown by ‘C’ in **a, b**



### 3.3 Relationship between the IIE's seesaw mode and summer precipitation anomalies

As the positive-anomaly and negative-anomaly patterns mirror each other to a large degree, we simply calculated the correlation coefficient to reveal the relationship between the IIE's seesaw mode and the summer precipitation (Fig. 7). In accordance with the anomalous atmospheric circulation patterns (Figs. 4, 5), there is stronger correlation between the IIE's seesaw mode and the summer precipitation over

the research domain. Significant positive correlation coefficients, with center values above 0.6, are found mainly over the northern Indian subcontinent, the western Indochina Peninsula, eastern Indochina Peninsula, Hainan Island, and the northern Philippines, suggesting that there is a stronger Indian summer monsoon and stronger SCS summer monsoon. Significant negative correlation coefficients, with center values below  $-0.6$ , are generally evident over the south and central Indian subcontinent, the lower and middle reaches of the Yangtze River, South Korea, and central Japan

**Fig. 5** As in Fig. 4, except for negative-anomaly years

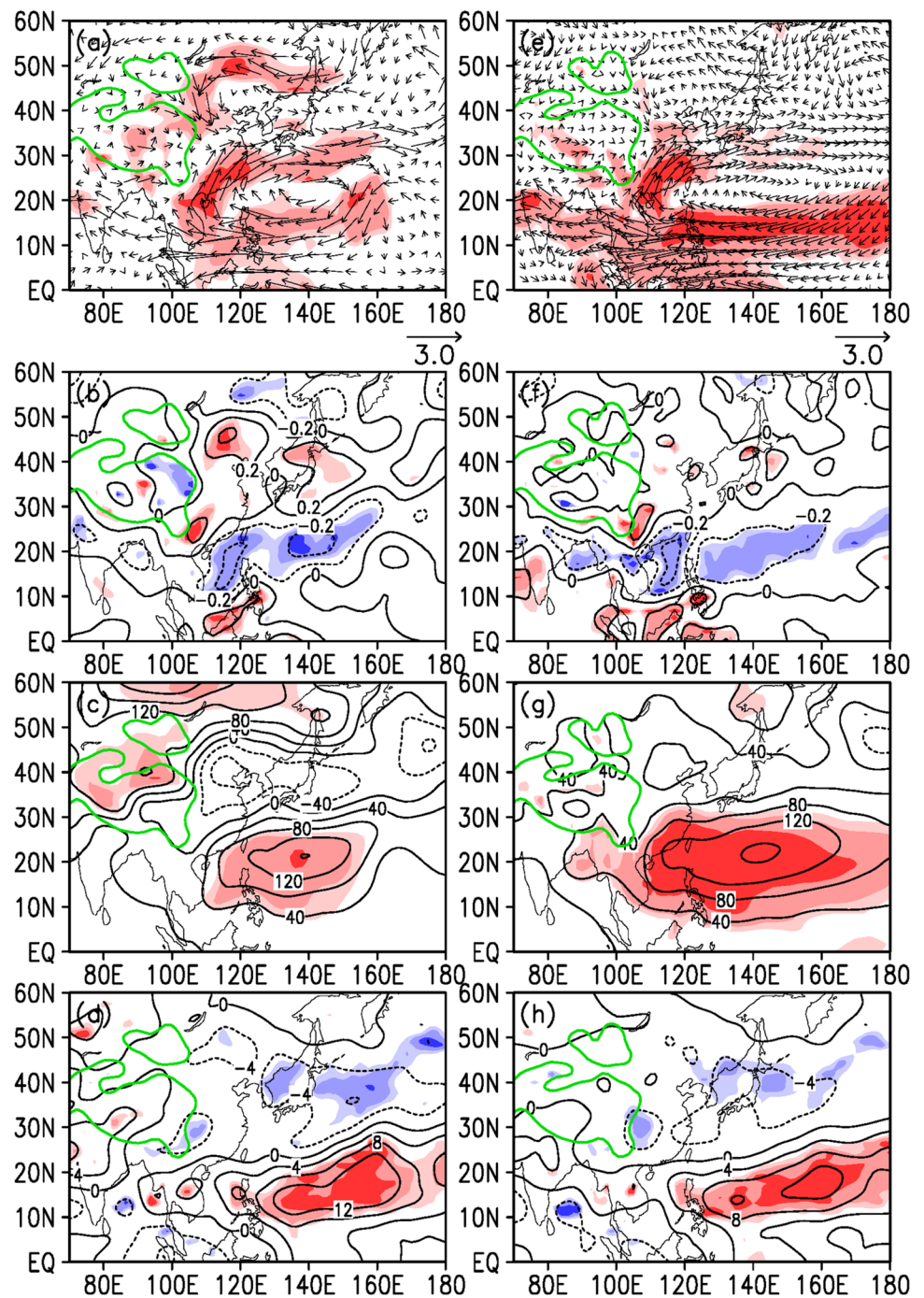


(Fig. 6), implying that there is a weaker subtropical summer monsoon over East Asia (the Mei-yu front). This means that, when the ISMT and SCSSMT are stronger (weaker) than normal, the IIE moves westward (eastward) in the area north of 22°N but shifts eastward (westward) in the area south of 22°N, and the summer precipitation is enhanced (reduced) over those positive correlation regions but reduced (enhanced) over the negative correlation areas. These results are consistent with previous studies (e.g., Qiao et al. 2002; Wang 2006; Wu et al. 2008; Huang et al. 2012).

### 3.4 Sea surface temperature anomalies associated with the IIE's seesaw mode

Many studies (e.g., Ju and Slingo 1995; Webster et al. 1998; Wu et al. 2003; Wang 2006; Huang et al. 2012) have demonstrated that the El Niño–Southern Oscillation (ENSO) is the dominant controller of the ASM. In El Niño years, with warmer SST anomalies (SSTAs) in the equatorial central-east Pacific, the monsoon circulation is weaker and its onset is later than normal. The opposite conditions occur in La

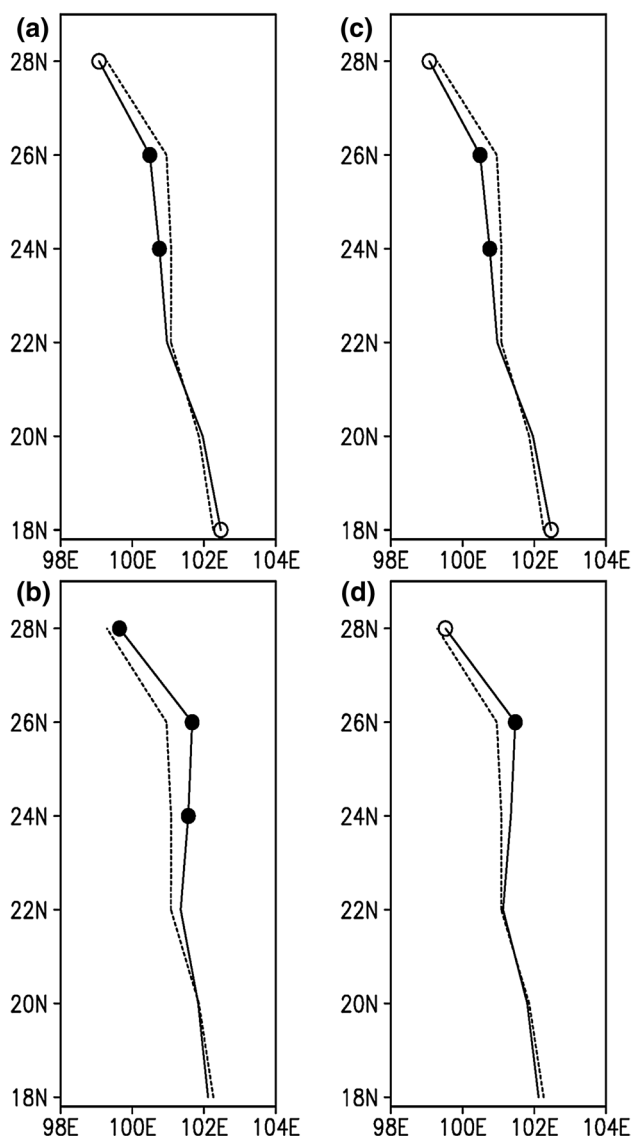


**Fig. 6** Position of the IIE in **a, c** positive-anomaly years and **b, d** negative-anomaly years. **a** and **b** are from NOAA-V2; **c** and **d** are from ERA-Interim. The dashed line denotes the normal position of the IIE

Niña years, with colder SSTAs in the equatorial central-east Pacific. Some recent studies have suggested that a persistent tropical Indian Ocean (TIO) warming may influence the summer monsoon through a discharging capacitor effect after El Niño has receded (e.g., Yang et al. 2007; Du et al. 2009; Xie et al. 2009). These studies imply that the SSTAs may influence the variability of the IIE's seesaw mode. Figure 8a, b show the correlation coefficients between the IIE's seesaw mode and the DJF (December–January–February) SSTA or 850-hPa horizontal winds. The correlation coefficients exhibit a typical La Niña pattern: colder SSTAs in the tropical central-east Pacific and TIO and warmer SSTAs in the tropical western Pacific. The TIO is controlled by westerly anomalies, and the tropical central-east Pacific is

dominated by easterly anomalies at 850 hPa. The negative SSTAs become stronger in the TIO and extend to tropical western Pacific with westerly anomalies moving northward, but the negative SSTAs and easterly anomalies become weaker and disappear in the tropical central-east Pacific from DJF to JJA (Fig. 8c, e or d, f). The corresponding lagged correlation coefficients between the IIE's seesaw mode, the Niño3.4 index (the SSTA averaged over the region 5°S–5°N, 170°–120°W), and the TIO index (the SSTA averaged over the TIO, 5°S–5°N, 50°–95°E) are also calculated (Fig. 8g). The significant negative correlation between the Niño3.4 index and the IIE's seesaw mode first appears in the previous November, and then persists into April. The significant negative correlation between the TIO index and the IIE's seesaw mode appears 1 month later than with the Niño3.4 index, but can persist to September, with the largest value in an absolute sense (below  $-0.5$ ) in May.

The results in Fig. 8 can be explained satisfactorily by the TIO capacitor effect (Xie et al. 2009). When an El Niño event develops in JJA, matures in DJF, and degenerates in the MAM (March–April–May) of the next year, it results in an anomalous anticyclone over the Northwestern Pacific. The anomalous anticyclone further induces warmer SSTAs persisting into JJA of the next year over the TIO basin. The warmer SSTAs over the TIO basin in turn maintain the anomalous anticyclone accompanied by suppressed rainfall over the Northwestern Pacific. Finally, the anomalous anticyclone weakens the ISMT and SCSSMT (Fig. 5). Under such anomalous circulation, the IIE moves eastward in the area north of 22°N but shifts westward in the area south of 22°N. When a La Niña occurs, the conditions are opposite, and the IIE moves westward in the area north of 22°N but shifts eastward in the area south of 22°N (Fig. 4).

### 3.5 Relative contributions of the SCSSMT and ISMT to the variability of the IIE's seesaw mode

The definition of the IIE (Cao et al. 2012) together with the results shown in Figs. 3, 4 and 5 imply that the variability of either of the two summer monsoon troughs will directly influence the IIE's variability. We can obtain the relative contributions of the ISMT and SCSSMT to the IIE through analyzing their synchronous correlation coefficients. We investigate the correlation for both reanalyses. Because the relative vorticity at 850 hPa can also reflect the intensity of the monsoon trough (Pan and Li 2006; Krishnamurti et al. 2013), we adopt the relative vorticity averaged over the rectangle C1 (16°–26°N, 76°–96°E) as an index of the intensity of the ISMT, and that averaged over rectangle C2 (10°–22°N, 108°–120°E) as an index of the intensity of the SCSSMT (Fig. 3). We denote the normalized time series of these indices from NOAA<sub>1,2</sub>-V2 over rectangles C1 and C2 as  $x_{1,1}$  and  $x_{1,2}$ , and those from ERA-Interim over rectangles C1 and C2 as  $x_{2,1}$  and  $x_{2,2}$ . The



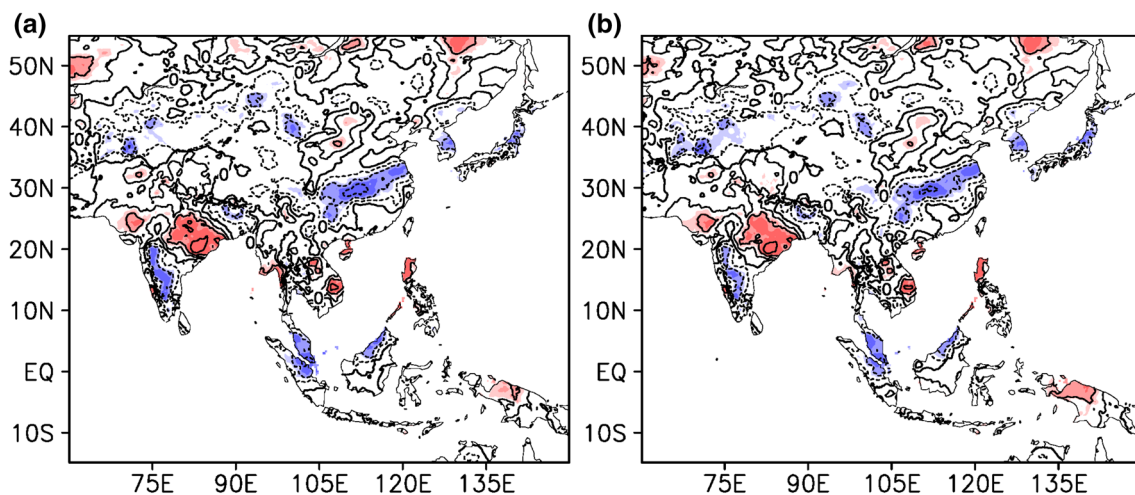


**Fig. 7** Correlation coefficients between the IIE's seesaw mode and summer precipitation calculated using **a** NOAA-V2 and **b** ERA-Interim. The areas shaded from light to dark denote correlation coef-

ficients passing the significance test at the 90%, 95% and 99% confidence level, respectively

dependent variable [the normalized time series of the left (IIE) canonical correlation field] associated with NOAA-V2 is written as  $y_1$ , and that associated with ERA-Interim as  $y_2$ . We first validated each set of results by calculating the corresponding correlation coefficients between the NOAA-V2 and ERA-Interim values. The correlation coefficients was 0.98 between the two indices associated with the IIE's seesaw mode, 0.81 between the two series averaged over rectangle C1, and 0.91 between the two series averaged over rectangle C2, passing the significance test at the 99.9% confidence level (Fig. 9a, b). The implication is that the results obtained by the two reanalysis datasets are reliable. The fact that the normal correlation coefficient set between the dependent and independent variables in Table 1 passed the significance test at the  $\geq 95\%$  confidence level suggests that the ISMT and SCSSMT are truly related to the IIE's variability, which is also consistent with the results obtained in Figs. 3, 4, 5 and 6.

To further obtain their relative importance, we calculated the relative contribution of the variances of the ISMT and SCSSMT to the IIE's variability (Table 2). Table 2 shows that the ISMT contributes 0.98% (1.76%), and the SCSSMT contributes 41.40% (44.06%) to the total variance of the IIE seesaw mode in NOAA-V2 (ERA-Interim). These results, which agree with the partial correlation coefficients (Table 1), indicate that the variability of the SCSSMT is more closely related than the ISMT to the IIE seesaw mode.

## 4 Summary

Using NOAA-V2 and ERA-Interim data, and EOF-CCA diagnostics, we have found that there is a seesaw mode of IIE variability. The seesaw mode of the IIE is characterized

by the northern part of the IIE moving westward (eastward) and the southern part moving eastward (westward), with a latitudinal node at around  $22^\circ\text{N}$ . The seesaw mode of the IIE is closely related to the in-phase variation of the IMST and SCSSMT. When the IMST and SCSSMT are stronger than normal, the IIE deviates from its normal position in an anticlockwise direction, with a center at around  $22^\circ\text{N}$ . When the IMST and SCSSMT are weaker than normal, roughly the opposite conditions will occur. This relationship has been verified by performing composite analysis on other variables: horizontal winds at 850 hPa, relative vorticity at 850 hPa, SLP, and OLR.

The IIE's seesaw mode is an efficient indicator of rainfall over the Asian monsoon area. When the IIE rotates in an anticlockwise direction, the rainfall over the Indian summer monsoon region and SCS summer monsoon region is heavier than normal, but the rainfall from the middle and lower reaches of the Yangtze River northeastward to central Japan is weaker than normal. When the IIE turns in a clockwise direction, an almost opposite pattern occurs. Since the IIE is the product of the interaction between the ISMT and SCSSMT to a larger degree, the thermal conditions of the Indian and Pacific oceans have a significant impact upon the variability of the IIE's seesaw mode. There is significant negative correlation between the east-central Pacific SST and the IIE's seesaw mode, persisting from the autumn of the previous year to the spring of the current year. Compared with the relationship between east-central Pacific SST and the IIE's seesaw mode, the significant negative correlation between TIO SST and the IIE's seesaw mode has a longer duration, beginning from the previous winter and lasting to the current summer, and has a much stronger correlation intensity. The TIO SST anomaly is one of the important

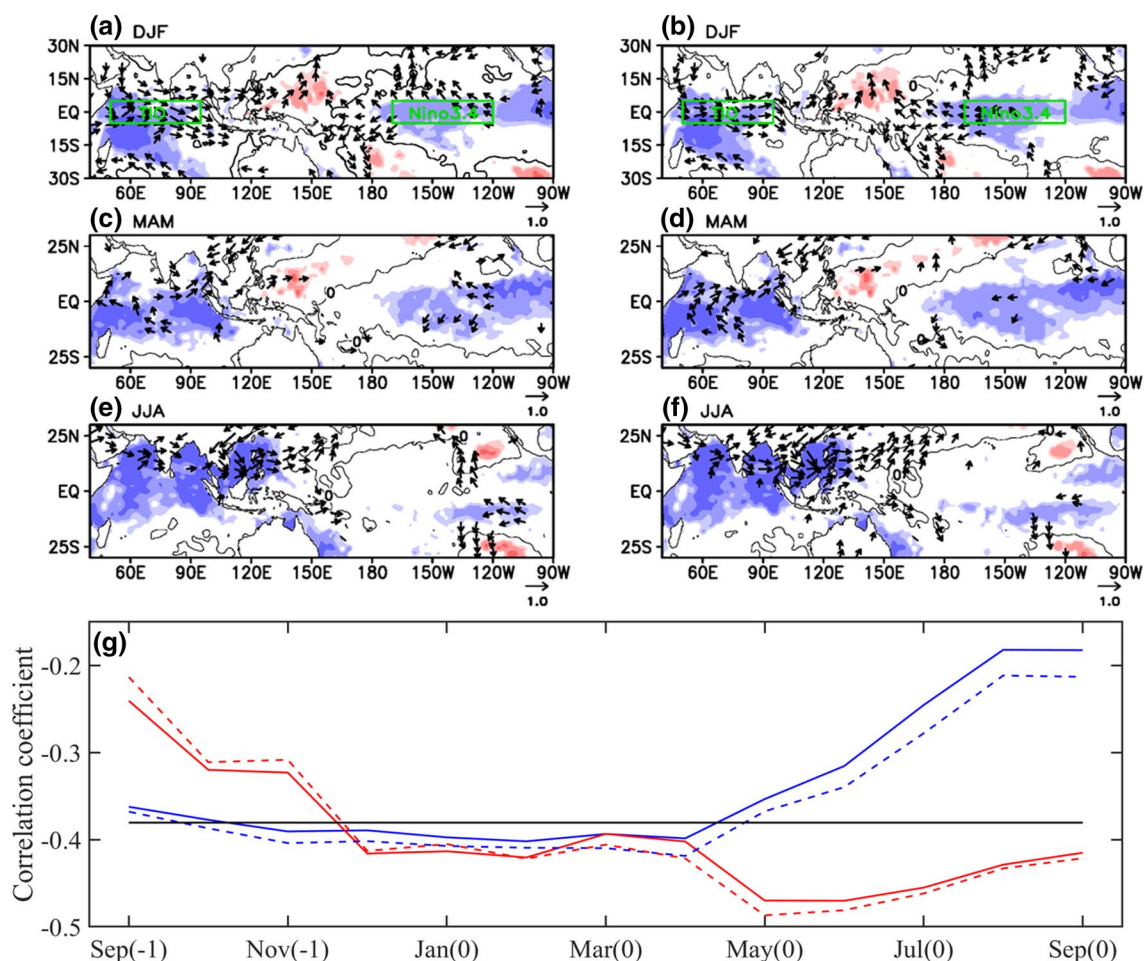


**Fig. 8** Correlation coefficients between the IIE's seesaw mode and DJF SST and 850-hPa horizontal winds calculated using **a** NOAA-V2 and **b** ERA-Interim. **c**, **e** Are the same as **a** but associated with SST and 850-hPa horizontal winds averaged in MAM and JJA. **d**, **f** are the same as **b** but associated with SST and 850-hPa horizontal winds averaged in MAM and JJA. In **a–f**, horizontal winds passing significance test at the 95% confidence level are shown, and the areas shaded from light to dark denote correlation coefficients passing the

significance test at the 90%, 95%, and 99% confidence level, respectively. **g** Coefficients of lagged correlation between the Niño3.4 index and the IIE's seesaw mode (blue lines) and between the TIO index and the IIE's seesaw mode (red lines). Colored solid (dashed) lines are obtained using NOAA-V2 (ERA-Interim). The black solid line denotes the critical value that passes the significance test at the 95% confidence level. (– 1) denotes the previous year, and (0) denote the current year

factors controlling the variability of the IIE's seesaw mode, through its influence over the two monsoon troughs over India and the SCS.

The relative degree of correlation between the IIE's seesaw mode, the ISMT and SCSSMT was further investigated by calculating their variance contributions. The SCSSMT is the primary factor influencing the IIE seesaw mode. The joint effect of the SCSSMT and ISMT, in which the effect of the ISMT on the IIE seesaw mode is mainly realized through the SCSSMT, is the second most important. Lastly, there is the effect of the ISMT only. Therefore, it is suggested that the SCSSMT plays a crucial role in the evolution of the IIE seesaw mode.

Cao et al. (2012) found that the IIE shifts farther east (west) than normal under a strong (weak) EASM and

weak (strong) ISM. Their results suggest that the IIE has an important feature; namely, that it tends to move toward cyclonic circulation. The seesaw mode of the IIE also reproduces this important feature. A stronger-than-normal ISMT and SCSSMT implies that there are stronger cyclonic anomalies over north-central India ( $16^{\circ}$ – $26^{\circ}$ N,  $76^{\circ}$ – $96^{\circ}$ E) and the SCS ( $10^{\circ}$ – $22^{\circ}$ N,  $108^{\circ}$ – $120^{\circ}$ E) in summer (Figs. 3, 4). Because the ISMT is located northwest of the SCSSMT, the  $5^{\circ}$  latitudinal difference between the two summer monsoon troughs happens to result in the IIE deviating from its normal position in an anticlockwise direction; i.e., the north part of the IIE moves toward the stronger cyclonic anomalies over north-central India, but its south part moves toward the stronger cyclonic anomalies over the SCS. On the contrary, when the ISMT and SCSSMT are weaker

**Fig. 9** **a** Normalized time series of the IIE (bars), relative vorticity averaged in rectangle C1 (blue line) and relative vorticity averaged in rectangle C2 (red line) using NOAA-V2. **b** is the same as **a** but using ERA-Interim

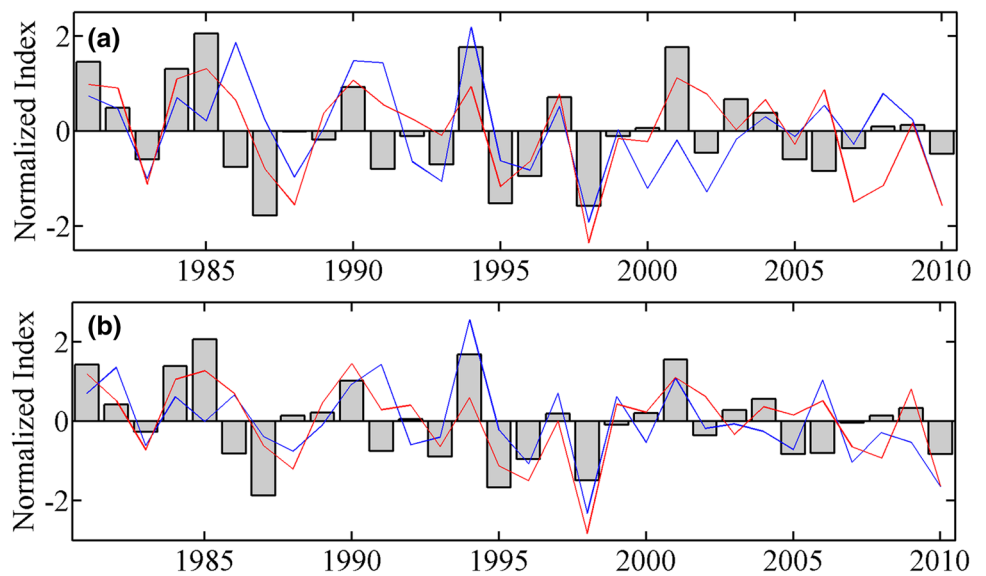


**Table 1** Correlation coefficients and partial correlation coefficients of (a)  $y_1$ ,  $x_{1,1}$ , and  $x_{1,2}$  calculated using NOAA-V2 and (b)  $y_2$ ,  $x_{2,1}$ , and  $x_{2,2}$  calculated using ERA-Interim

| (a)       | $y_1$   | $x_{1,1}$ | $x_{1,2}$ |
|-----------|---------|-----------|-----------|
| $y_1$     | 1.000   | 0.420*    | 0.651***  |
| $x_{1,1}$ | 0.024   | 1.000     | 0.623***  |
| $x_{1,2}$ | 0.548** | –         | 1.000     |
| (b)       | $y_2$   | $x_{2,1}$ | $x_{2,2}$ |
| $y_2$     | 1.000   | 0.498**   | 0.677***  |
| $x_{2,1}$ | 0.033   | 1.000     | 0.711***  |
| $x_{2,2}$ | 0.528** | –         | 1.000     |

Values above the main diagonal are normal correlation coefficients, and values below are partial correlation coefficients

\*Correlation coefficients passing the significance test at the 95% confidence level

\*\*Correlation coefficients passing the significance test at the 99% confidence level

\*\*\*Correlation coefficients passing the significance test at the 99.9% confidence level

than normal, stronger anticyclonic anomalies develop over the north of the Bay of Bengal and the SCS in summer (Figs. 4, 5, 6). Stronger cyclonic anomalies appear from south India to south of the Bay of Bengal, and north of the western North Pacific subtropical high. The latitudinal difference between the two cyclonic anomalies results in the IIE deviating from its normal position in a clockwise direction. Therefore, the latitudinal difference between the two monsoon troughs may be an important driver of the seesaw mode of the IIE.

Seasonal forecasting of the Indian and East Asian summer monsoons has always been a key issue in short-term

**Table 2** Relative variance contribution (%) of the (a) ISMT ( $x_{1,1}$ ) and SCSSMT ( $x_{1,2}$ ) calculated from NOAA-V2 and (b) ISMT ( $x_{2,1}$ ) and SCSSMT ( $x_{2,2}$ ) calculated from ERA-Interim

| Variable                  | $x_{1,1}$ | $x_{1,2}$ |
|---------------------------|-----------|-----------|
| (a)                       |           |           |
| Variance contribution (%) | 0.98      | 41.40     |
| Variable                  | $x_{2,1}$ | $x_{2,2}$ |
| (b)                       |           |           |
| Variance contribution (%) | 1.76      | 44.06     |

climate prediction over Asia, because the two subsystems of the ASM significantly influence the livelihood of the local population (Wang 2006 and references cited therein). The seesaw mode of the IIE is closely related to the ISMT and SCSSMT and significantly correlated with the SSTA in the preceding months over the TIO and tropical east-central Pacific. Therefore, it can be used as a predictor in the seasonal forecast of the Indian summer monsoon and East Asian summer monsoon. When the IIE deviates from its normal position in an anticlockwise (a clockwise) direction, more (less) than normal summer monsoonal rainfall might be predicted over the north-central Indian subcontinent and South China Sea, but less (more) than normal summer monsoonal rainfall might be predicted in the low and middle reaches of the Yangtze River–South Korea–central Japan.

The East Asia–Pacific (EAP) teleconnection identified by Huang and Li (1987) or the Pacific–Japan (PJ) teleconnection reported by Nitta (1987) is closely related to the IIE seesaw mode (Figs. 4, 5, 6, 7). Recently, Gong et al. (2018) found that the amplitude of the western North Pacific center of the EAP or PJ teleconnection is influenced mainly by the SSTAs and local air–sea feedback over the

same region in CMIP5 (Phase 5 of the Coupled Model Intercomparison Project) models. Their results suggest that the SSTAs and local air–sea feedback over the western North Pacific may also regulate the variability of the IIE seesaw mode. Xu et al. (2019) found that the PJ pattern presents a significant three-dimensional structural change in the late 1990s. Cao et al. (2012) and Tao et al. (2016) found that the WPSH is the main driver of the zonal movement of the entire IIE. The seesaw mode of the IIE, found in this study, is also closely related to the WPSH (Figs. 4, 5). The results imply that the westward ridge point of WPSH (Yang et al. 2017) may influence the IIE variability via its position and shape. We will study these interesting issues in future work.

**Acknowledgements** This work was supported by the National Natural Science Foundation of China (4181101147, 41875103 and 41565002), the program for Innovative Research Team in Science and Technology in University of Yunnan Province, the Natural Science Foundation of Yunnan Province (2018FY001-018, 2018FB081, and 2018BC007), and Science and Technology Project of Yunnan Province (2016RA096).

## References

- Barnett TP, Preisendorfer R (1987) Origins and levels of monthly and seasonal forecast skill for United States surface air temperatures determined by canonical correlation analysis. *Mon Weather Rev* 115:1825–1850
- Busuioac A, Giorgi F, Bi X, Ionita M (2006) Comparison of regional climate model and statistical downscaling simulations of different winter precipitation change scenarios over Romania. *Theor Appl Climatol* 86:101–123
- Busuioac A, Tomozeiu R, Cacciamani C (2008) Statistical downscaling model based on canonical correlation analysis for winter extreme precipitation events in the Emilia-Romagna region. *Int J Climatol* 28:449–464
- Cao J, Hu JM, Tao Y (2012) An index for the interface between the Indian summer monsoon and the East Asian summer monsoon. *J Geophys Res* 117:D18108. <https://doi.org/10.1029/2012JD017841>
- Compo GP, Whitaker JS, Sardeshmukh PD (2006) Feasibility of a 100 year reanalysis using only surface pressure data. *Bull Amer Meteorol Soc* 87:175–190
- Compo GP, Whitaker JS, Sardeshmukh PD, Matsui N, Allan RJ, Yin X, Gleason BE, Vose RS, Rutledge G, Bessemoulin P, Brönnimann S, Brunet M, Crouthamel RI, Grant AN, Groisman PY, Jones PD, Kruk M, Kruger AC, Marshall GJ, Maugeri M, Mok HY, Nordli Ø, Ross TF, Trigo RM, Wang XL, Woodruff SD, Worley SJ (2011) The twentieth century reanalysis project. *Q J R Meteorol Soc* 137:1–28
- Dee DP, Uppala SM, Simmons AJ, Berrisford P, Poli P, Kobayashi S, Andrae U, Balmaseda MA, Balsamo G, Bauer P, Bechtold P, Beljaars A C M, van de Berg L, Bidlot J, Bormann N, Delsol C, Dragani R, Fuentes M, Geer AJ, Haimberger L, Healy SB, Hersbach H, Hólm EV, Isaksen I, Kållberg P, Köhler M, Matricardi M, McNally AP, Monge-Sanz BM, Morcrette J-J, Park B-K, Peubey C, de Rosnay Tavolato P, Thépaut JN, Vitart F (2011) The ERA-Interim reanalysis: configuration and performance of the data assimilation system. *Q J R Meteorol Soc* 137:553–597
- Ding YH, Li CY, He JH, Chen LX, Gan ZJ, Qian YF, Yang JY, Wang DX, Shi P, Fan WD, Xu JP, Li L (2004) South China Sea Monsoon Experiment (SCSMEX) and the East Asian Monsoon (in Chinese). *Acta Meteorol Sin* 62:561–586
- Du Y, Xie SP, Huang G, Hu KM (2009) Role of air–sea interaction in the long persistence of El Niño-induced North Indian Ocean warming. *J Clim* 22:2023–2038
- Gong HN, Wang L, Chen W, Wu RG, Huang G, Debashis N (2018) Diversity of the Pacific–Japan Pattern among CMIP5 Models: role of SST anomalies and atmospheric mean flow. *J Clim* 31:6857–6877
- He JH, Wang LJ, Xu HM (2000) Abrupt change in elements around 1998 SCS summer monsoon establishment with analysis of its characteristic process. *Acta Meteorol Sin* 14:426–432
- Heyen H, Zorita E, von Storch H (1996) Statistical downscaling of monthly mean North Atlantic air-pressure to sea level anomalies in the Baltic Sea. *Tellus* 48A:312–323
- Huang RH, Li WJ (1987) Influence of the heat source anomaly over the western tropical Pacific on the subtropical high over East Asia. In: International conference on the general circulation of East Asia, pp 40–51
- Huang RH, Chen JL, Wang L, Lin ZD (2012) Characteristics, processes, and causes of the spatio-temporal variabilities of the East Asian monsoon system. *Adv Atmos Sci* 29:910–942
- Jin ZH, Chen LX (1982) On the medium-range oscillation of the East Asian monsoon circulation system and its relation with the Indian monsoon system. The National Symposium Collections on the Tropical Summer Monsoon (in Chinese). People’s Press of Yunnan Province, Yunnan, pp 204–215
- Jin Q, Yang XQ, Sun XG, Fang JB (2013) East Asian summer monsoon circulation structure controlled by feedback of condensational heating. *Clim Dyn* 41:1885–1897
- Ju JH, Slingo JM (1995) The Asian summer monsoon and ENSO. *Q J R Meteorol Soc* 121:1133–1168
- Kang I-S, Ho C-H, Lim Y-K, Lau KM (1999) Principal modes of climatological seasonal and intraseasonal variation of the Asian summer monsoon. *Mon Weather Rev* 127:322–340
- Kennedy JJ, Rayner NA, Smith RO, Saunby M, Parker DE (2011a) Reassessing biases and other uncertainties in sea-surface temperature observations since 1850 part 1: measurement and sampling errors. *J Geophys Res* 116:D14103. <https://doi.org/10.1029/2010JD015218>
- Kennedy JJ, Rayner NA, Smith RO, Saunby M, Parker DE (2011b) Reassessing biases and other uncertainties in sea-surface temperature observations since 1850 part 2: biases and homogenisation. *J Geophys Res* 116:D14104. <https://doi.org/10.1029/2010JD015220>
- Krishnamurthy V (2016) Intraseasonal oscillations in East Asian and South Asian monsoons. *Clim Dyn* 1:1–21
- Krishnamurti TN, Bhalme HN (1976) Oscillations of monsoon system. Part I: observational aspects. *J Atmos Sci* 33:1937–1954
- Krishnamurti TN, Stefanova L, Misra V (2013) Tropical meteorology, an introduction. Springer, New York, pp 75–120
- Liebmann B (1996) Description of a complete (interpolated) outgoing longwave radiation dataset. *Bull Amer Meteorol Soc* 77:1275–1277
- Lim YK, Kim KY, Lee HS (2002) Temporal and spatial evolution of the Asian summer monsoon in the seasonal cycle of synoptic fields. *J Clim* 15:3630–3644
- Nitta T (1987) Convective activities in the tropical western Pacific and their impact on the Northern Hemisphere summer circulation. *J Meteorol Soc Jpn* 65:373–390
- Pan J, Li CY (2006) Comparison of climate characteristics between two summer monsoon troughs over the South China Sea and India (in Chinese). *Chin J Atmos Sci* 30:377–390
- Qiao YT, Luo HB, Jian MQ (2002) The temporal and spatial characteristics of moisture budgets over Asian and Australian monsoon regions. *J Trop Meteorol* 8:113–120

- Tao Y, Cao J, Lan GD, Su Q (2016) The zonal movement of the Indian–East Asian summer monsoon interface in relation to the land–sea thermal contrast anomaly over East Asia. *Clim Dyn* 17:2759–2771
- Von Storch H, Zorita E, Cubasch U (1993) Downscaling of global climate change estimates to regional scale: an application to Iberian rainfall in wintertime. *J Clim* 6:1161–1171
- Wang B (2006) *The Asian monsoon*. Springer, Berlin
- Wang B, Lin H (2002) Rainy season of the Asian–Pacific summer monsoon. *J Clim* 15:386–398
- Wang B, Wu RG (1997) Peculiar temporal structure of the South China Sea summer monsoon. *Adv Atmos Sci* 14:177–193
- Wang B, Steven CC, Liu P (2003) Contrasting the Indian and East Asian monsoons: implications on geologic timescales. *Mar Geol* 201:5–21
- Webster PJ, Magaña VO, Palmer TN, Shukla J, Tomas RA, Yanai M, Yasunari T (1998) Monsoons: processes, predictability, and the prospects for prediction. *J Geophys Res* 103:14451–14510
- Whitaker JS, Compo GP, Wei X, Hamill TM (2004) Reanalysis without radiosondes using ensemble data assimilation. *Mon Weather Rev* 132:1190–1200
- Wu RG, Hu ZZ, Kirtman BP (2003) Evolution of ENSO-related rainfall anomalies in East Asia. *J Clim* 16:3742–3758
- Wu BY, Zhang RH, Ding YH, D’arrigo R (2008) Distinct modes of the East Asian summer monsoon. *J Clim* 21:1122–1138
- Xie SP, Hu K, Hafner J, Tokinaga H, Du Y, Huang G, Sampe T (2009) Indian Ocean capacitor effect on Indo-western Pacific climate during the summer following El Niño. *J Clim* 22:730–747
- Xu PQ, Wang L, Chen W, Feng J, Liu YY (2019) Structural changes in the Pacific–Japan pattern in the late 1990s. *J Clim* 32:607–621
- Yang J, Liu Q, Xie SP, Liu Z, Wu L (2007) Impact of the Indian Ocean SST basin mode on the Asian summer monsoon. *Geophys Res Lett* 34:L02708. <https://doi.org/10.1029/2006GL028571>
- Yang RW, Xie ZA, Cao J (2017) A dynamic index for the westward ridge point variability of the Western Pacific subtropical high during summer. *J Clim* 30:3325–3341
- Yatagai A, Kamiguchi K, Arakawa O, Hamada A, Yasutomi N, Kito A (2012) APHRODITE: constructing a long-term daily gridded precipitation dataset for Asia based on a dense network of rain gauges. *Bull Amer Meteorol Soc* 93:1401–1415
- Zhu QG, He JH, Wang PX (1986) A study of circulation differences between east Asian and Indian summer monsoons with their interaction. *Adv Atmos Sci* 3:466–477

**Publisher’s Note** Springer Nature remains neutral with regard to jurisdictional claims in published maps and institutional affiliations.